Experimental Realization of Coherent Perfect Polarization Rotation

CHUANHONG ZHOU[1], JAMES H. ANDREWS[1], AND MICHAEL CRESCIMANNO[1]

[1]Department of Physics and Astronomy, Youngstown State University, Youngstown, OH, 44555
*Corresponding author: dcphtn@gmail.com

Compiled April 1, 2016

Coherent perfect processes enable high optical efficiencies in optical conversion phenomena such as coherent perfect absorption or coherent perfect polarization rotation. A linear optical coherent perfect process based on Faraday rotation has been evaluated experimentally, achieving contrast limited by other optical components of the system and demonstrating like-parity resonance doublets above threshold.

OCIS codes: *(260.3160) Physical Optics;(030.1670) Coherent Effects; (160.3820) Magnetooptics*

http://dx.doi.org/10.1364/ao.XX.XXXXXX

Wave impedance mismatches at boundaries typically excite reflected waves that reduce the efficiency of optical processes. Reducing impedance mismatch at a boundary using anti-reflection layers is limited by the inability to tune anti-reflection layers post-fabrication. Thus, in design, one must typically compromise between increased optical bandwidth and improved impedance matching across that bandwidth.

As a previous example, Coherent Perfect Absorption (CPA, also called the anti-laser) addresses these issues in design by using multi-port interference and absorption processes (by nature, in part time-reversal odd, or non-reciprocal) simultaneously to eliminate light that would otherwise emerge from any / all of the device ports [1–8]. Absorption is not the only time-reversal-odd effect, however, to which the idea of a coherent perfect process applies. In Coherent Perfect Polarization Rotation (CPR) the combination of interference and Faraday rotation (notably also time-reversal odd) enhances the optical efficiency of the polarization conversion process at narrow band resonance peaks through control of the amplitude and phase of incoming beams [9–12]. As described in Ref. [9], CPR is a Hermitian and conservative optical process. It expands the range of applications for coherent perfect processes to include devices such as laser wavelength locks, field sensors, optical isolators, and optical modulators by both reducing the field-length product for Faraday rotation and enabling dynamic control *in situ* through changes to the relative phase of the input beams.

CPR in the linear two-port context can be conveniently described in terms of the symmetries of the usual field transfer matrices (for a modern review see [13]). We denote the field amplitudes at each location by complex-valued linear combinations of field vectors proportional to $e^{i(\pm kz+\omega t)}$, and work in the linear polarization basis $\vec{u} = (E_x, B_y, E_y, -B_x)$. The relation between field amplitudes at any two points is a linear map ($\mathbf{M}$, the transfer matrix) $\vec{u}(z') = \mathbf{M}(z', z)\vec{u}(z)$, which inherits the underlying symmetries of electromagnetism. The case of interest, assuming no linear birefringence along z, stipulates that $\mathbf{M} = \begin{bmatrix} M & C \\ -C & M \end{bmatrix}$ where M and C are 2×2 matrices further described below. Also, our system is parity symmetric, implying, that $M_{11} = M_{22}$ and $C_{11} = C_{22}$. In this basis, the time reversed transfer matrix ij'th matrix element is $(-1)^{i+j}M_{ji}$. Using parity we can then decompose the field space into parity-even and parity-odd sectors. For simplicity, we discuss only the field parity-even resonances here, the odd parity following a parallel argument. For a parity-even state (i.e., light incident on both sides of a homogeneous rotator with no phase difference across it) calculation shows that the amplitude of the outgoing unrotated light is proportional to $(1,1)C^{-1}(M-P)\begin{pmatrix}1\\1\end{pmatrix}$, where P is the 2×2 parity matrix with elements $P_{ij} = (-1)^{i+1}\delta_{ij}$, where $i, j = 0, 1$.

Finally, we impose power conservation, from which we learn that, for M to be time-reversal even, C is proportional to M. From the above expression, the unrotated light amplitude in this case is thus proportional to $(2 - M_{12} + M_{21})$ and can never be zero, as M_{12} and M_{21} are purely imaginary. Taking the case of time-reversal odd transport, but again imposing power conservation, leads to three branches of solutions for C. One of these solutions is the familiar one of Faraday rotation in a dielectric, but each solution has the form $M = \begin{bmatrix} \mathcal{R} & \mathcal{I} \\ \mathcal{I} & \mathcal{R} \end{bmatrix}$ and, $C = \begin{bmatrix} \mathcal{I} & \mathcal{R} \\ \mathcal{R} & \mathcal{I} \end{bmatrix}$, where $\mathcal{R}$ and $\mathcal{I}$ are purely real or purely imaginary, respectively. When these are used in the expression for the amplitude of the unrotated light, $(1,1)C^{-1}(M-P)\begin{pmatrix}1\\1\end{pmatrix}$,

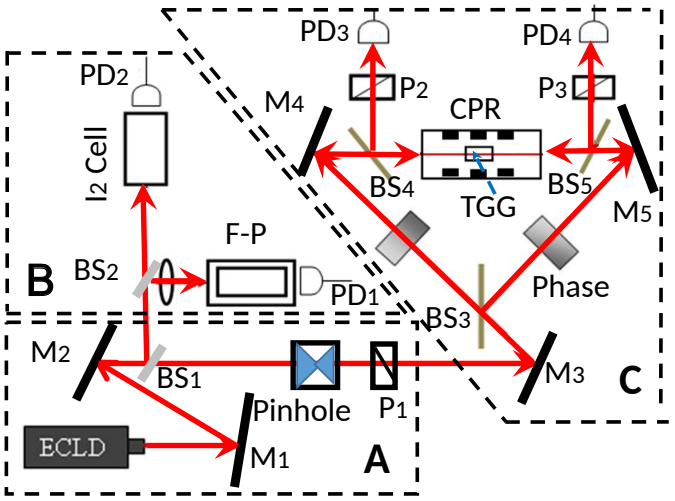

Fig. 1. Experimental schematic. Rectangle A shows the beam conditioning optics, trapezoid B shows the laser frequency monitoring optics, and trapezoid C shows the triangular interferometric polarization conversion setup. Here, M=mirror, Bs=beamsplitter, P=polarizer / analyzer, PD=photodetector, F-P=Fabry-Perot interferometer, and I_2 Cell=Iodine cell for referencing the laser frequency.

one sees the wavelength and the magnitude of the time-reversal odd piece can be chosen to force this (complex) polarization amplitude to zero. Then, by power conservation and parity, all light emerging from the system must have the orthogonal polarization. [9] Thus, the CPR state is achieved when the reflected and transmitted components in the input polarization destructively interfere *simultaneously on both sides*. As the magnetic field increases, the transmitted portion in the original polarization decreases. At threshold field the magnitude of the reflected and transmitted light in the input polarization are identical so interferometric extinction is possible on the sample's 'cavity' resonance. At higher magnetic fields, since C and M depend locally linearly on the detuning, the CPR condition above becomes a quadratic equation with two real roots, resulting in like-parity CPR resonance doublets. Beyond this simple example, theory [10] indicates CPR states exist in more complex nonreciprocal optical systems including isolators and modulators.

We report here on a first experimental demonstration of CPR as shown by the change of optical contrast above threshold and by the CPR resonances appearing in like-parity doublets. Our experiment uses an external cavity diode laser (ECLD) at 658nm in a 1.4 cm long terbium gallium garnet (TGG , index of refraction 1.9 at 658nm) slab immersed in a magnetic field, as in the proof-of-principle experiment described in last section of Ref. [9]. As detailed in Fig. 1, the light emerges from a ECLD (laser linewidth < 1 MHz) and, after spatial filtering, is sent into a triangular interferometer. Because the input light's phase difference across the TGG slab is a key parameter, we employ a DC-driven $LiNiO_3$ phase modulator in one arm. A continuously variable attenuator is adjusted to balance the lightfield intensities, post modulator, in the interferometer's arms. The light is then steered with dielectric polarization preserving mirrors into the facets of the TGG slab mounted inside a hollow Pyrex pipe inside a permanent magnet assembly. The magnet assembly consists of three commercially available annular rare earth magnets [14] with like poles facing each other, held

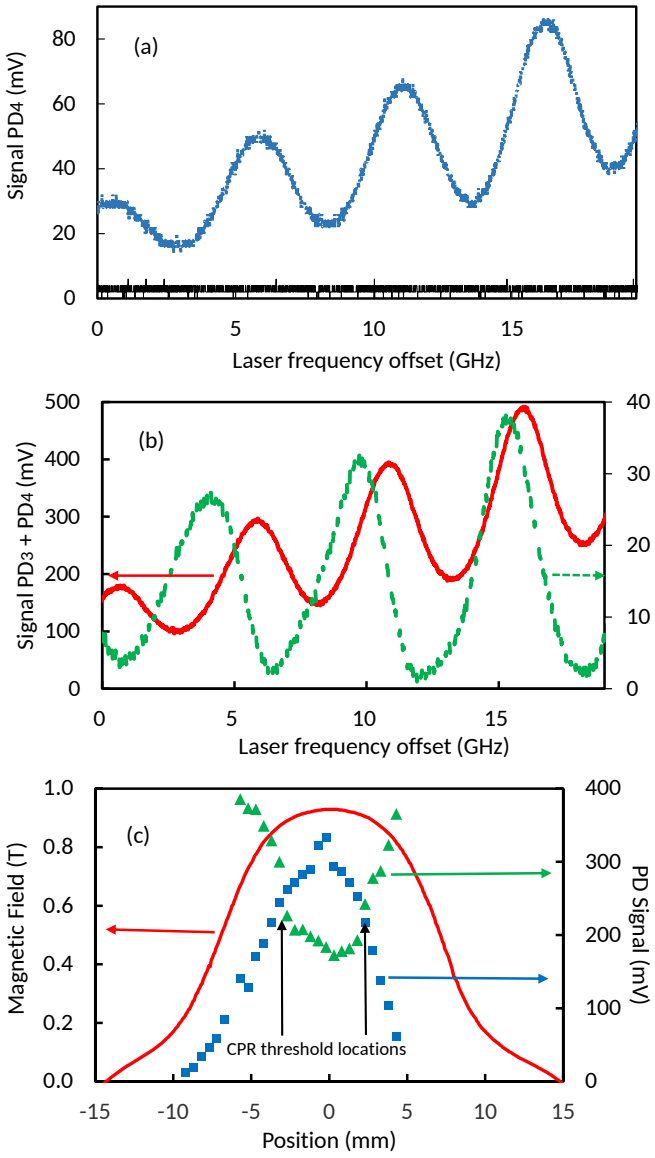

Fig. 2. (a) Etaloning in transmission signal (blue dotted curve) from a single input field (lower thin black line is dark signal), and (b) typical summed intensity arising from two counter-propagating fields in the low field ($<$ 0.05 T) case (red, solid, scale left) and at a sample-averaged field of $\sim$ 0.85 T (green, dashed, scale right), showing both the overall reduction in the emerging light at the input polarization with increased field and the extinctions in the sum signal at larger field, the basic CPR process. (c) axial field map (red, solid) and transmitted (green, triangles) and reflected (blue, squares) single beam intensities as a function of the TGG (length 14mm) sample's center, showing $\sim$ 7mm region with field above CPR threshold.

concentric and compressed longitudinally inside an aluminum tube. In this arrangement, a magnetic field maximum ($\sim$ 0.92 T) occurs inside the center bore of the middle magnet. At that center location the sample-averaged field is 0.85 T. The magnets and magnet holder are mounted on a linear track so that the entire magnet assembly can be moved relative to the TGG slab (the ends of the Pyrex pipe extend to mounts beyond the track).

Finally, light that emerges from both sides of the TGG slab is

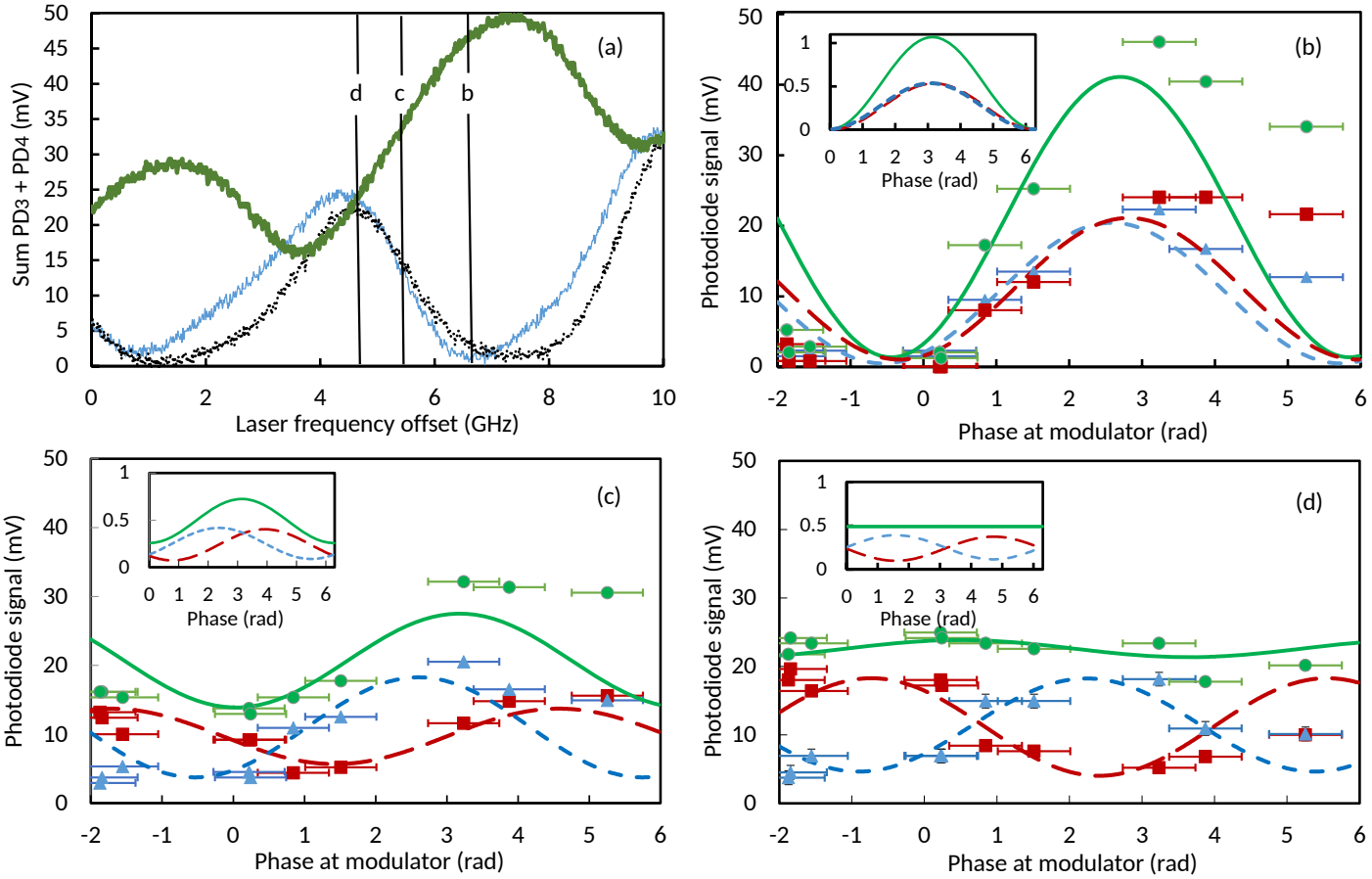

Fig. 3. (a) Examples of three laser frequency sweeps with different phase shifts between the counter-propagating beams. (b), (c), and (d) show the measured (red squares, blue triangles) and fit (long dash-red, short dash-blue) phase dependence of the individual traces and the summed trace (green circles) and fit (solid green line) for each of the three laser frequency offsets shown in Fig. 3(a). The insets in Figs. 3(b), (c) and (d) show corresponding theoretically predicted values for the case of slightly mismatched beam intensities (1:1.2) using the same color and line type scheme as the fits.

sampled using non-polarizing beam splitters BS_4 and BS_5 and sent to polarization analyzers P_2 and P_3 (extinction coefficient in the 100's) and onto a matched pair of 1 cm^2 amplified photodiodes PD_3 and PD_4. The polarizers P_2 and P_3 are carefully aligned with the original optical field's polarization. Thus the graphs in Figs. 2 and 3 indicate light of the same polarization as the input field.

The TGG slab's facets are optically flat and parallel enough that etaloning is readily discernible in the transmission graph of a single beam (see Fig. 2(a)) during a laser frequency sweep. When this light is simultaneously incident on the TGG slab as counter-propagating fields at low magnetic field the summed photodiode signal is that of the red solid trace in Fig. 2(b). This is reminiscent of the single beam graph, though there is wave interference at each photodiode. The green dashed trace in Fig. 2(b) is the typical summed signal from counter-propagating fields when the TGG slab is in a large longitudinal magnetic field. (In both (a) and (b) the intensity's linear envelope is an artifact of the sweep method.)

That the high magnetic field curve at certain frequencies is much closer to extinction than the low-field curve indicates the onset of CPR. Note that Fig. 2(b) is the raw data and that the phase difference across the TGG slab varies during the laser frequency sweep so that this trace does not correspond exactly to the actual optimal phase (0 or π for this simple parity-symmetric slab system) for CPR resonance at any of the high-field minima. Moving the magnet assembly subjects the TGG to different magnetic fields. For single-side illumination, when the intensities of the reflected and transmitted light in the same polarization state as the input light become equal, as shown in Fig. 2(c), the threshold for then achieving CPR with two counter-propagating beams is reached. Note that at that threshold location the sample averaged field (over the 14mm long specimen) is close to the theoretically expected 0.65 T for TGG[9]. Once above threshold (all high field data described here were taken with the TGG center near the field maximum, leading to a sample-averaged field of about 0.85 T), CPR resonances occur slightly below and above the etaloning minima, comprising like-parity doublets as anticipated in [9].

Procedurally, to delineate the full dependence on the phase difference across the TGG crystal, we record these laser sweeps for 10 different phase retardations from the phase modulator. In Fig. 3, we graph the individual and summed photodetector signals as a function of the phase retardation both on resonance (Fig. 3(b), using the location marked 'b' in Fig. 3(a)), slightly off resonance (Fig. 3(c) and using the location marked 'c' in Fig. 3(a)), and far off resonance (Fig. 3(d), and at the location marked 'd' in Fig. 3(a)). The sums of these signals ap-

pear as green circles. The lines are best three-parameter fits as a sum of a constant term and a sinusoid in the modulator phase. The insets in these figures are the associated idealized theoretical curves for the individual photodiode signals and their sum, indicating throughout, the same pattern of alignment on resonance and misalignment off resonance. We note the similarity of these to the signals found for the same detunings in a CPA experiment (see Fig. 2 of Ref. [2]).

Finally, in Fig. 4 we display the experimentally measured contrast (max / min) of the sum signal versus laser detuning. To find the maximum and minimum at each laser detuning, we interpolated between the 10 phase offsets to find a phase and light signal at that phase that would correspond to either a maximum or a minimum. Because there is a stable, but frequency-dependent, phase offset at each detuning, we are not able to measure independently the absolute phase difference of the incoming lightfields across the TGG plate. The two traces in Fig. 4(a) are contrast maxima (with respect to modulator phase) for each laser detuning at small magnetic field (inset) and at a field above the CPR threshold. Although at small magnetic fields the contrast only varies between 1.2 and 1.9, at magnetic fields above threshold the contrast can be quite large. The expected doublet structure is also evident in the graph. Between doublets (off resonance) the contrast can be as low as the low magnetic field case, suggesting the application of CPR contrast enhancement as a polarization output phase switch. In Fig. 4(b), we include corresponding theoretical curves for qualitative comparison. To prepare Fig. 4(b), we chose the ratio of intensities of the output beams to be 0.81, took the phase difference across the TGG plate faces to be 0.1 rad (rather than 0 or π) and also introduced a difference in the detector sensitivity just to indicate how laboratory nonideality create asymmetries in the experimental contrast curves.

Our experiments unambiguously demonstrate narrow band coherent perfect polarization rotation in its most basic implementation and in quantitative agreement with CPR theory. The data show strong phenomenological correspondences with other coherent perfect processes such as CPA. Further experimental work is focused on lowering the required magnetic field-length product by using layered materials and / or by combining Faraday rotation with optical activity, all as further described theoretically in Ref. [10].

Funding. National Science Foundation (NSF) (ECCS-1360725); The Science and Technology Center for Layered Polymeric Systems, National Science Foundation (NSF) (DMR 0423914).

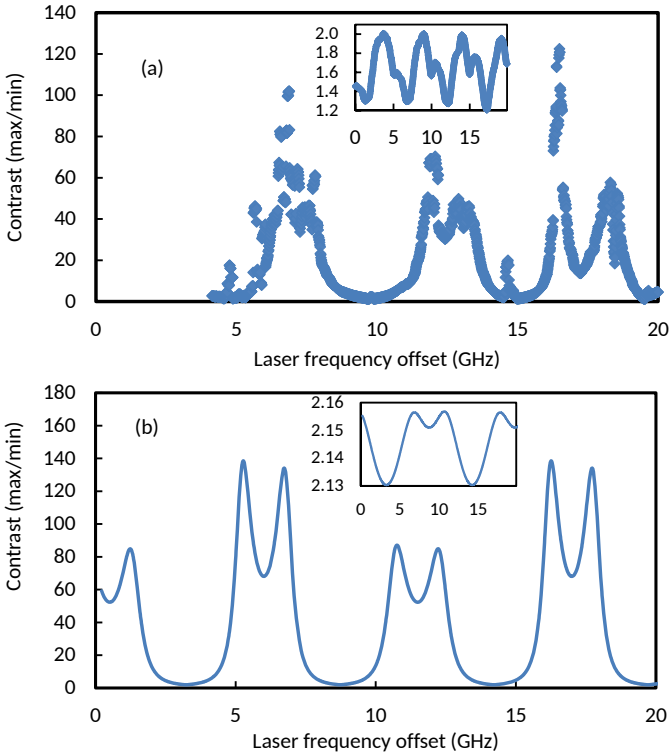

Fig. 4. The extinction ratio of the CPR resonances(a) experiment and (b) theory. Note that there are twice as many resonances as the expected FSR of the crystal, indicating the 'magnetic doublet' nature of the CPR resonances. Note also that the extinction ratio is essentially limited chiefly by the coherence of our laser source. (For example, in a Mach-Zehnder interferometer this laser's measured fringe contrast (max-min) / avg was greater than 95%.) For comparison, the insets in each figure show the low field response.

REFERENCES

1. Y. D. Chong, L. Ge, H. Cao, and A. D. Stone, Phys. Rev. Lett., **105**, 053901 (2010).
2. W. Wan, Y. Chong, L. Ge, H. Noh, A. D. Stone, and H. Cao, Science, **331**, 889 (2011).
3. S. Longhi, Phys. Rev. A **83**, 055804 (2011).
4. S. Dutta-Gupta, O. J. F. Martin, S. Dutta Gupta, and G. S. Agarwal, Opt. Express **20**, 1330 (2012).
5. S. Dutta-Gupta and G. S. Agarwal, Opt. Lett. **39**, 390 (2014).
6. S. Longhi and G. D. Valle, Phys. Rev. A **85**, 053838 (2012).
7. K. N. Reddy and S. D. Gupta, Opt. Lett. **38**, 5252 (2013).
8. S. Longhi, Opt. Lett. **40**, 1278 (2015).
9. M. Crescimanno, N. J. Dawson, and J. H. Andrews, Phys. Rev. A., **86**, 031807(R) (2012).
10. M. Crescimanno, C. Zhou, J. H. Andrews and M. A. Baker, Phys. Rev. A **91**, 013845 (2015).
11. Y. Wang, M. Pu, C. Hu, Z. Zhao, C. Wang, and X. Luo, Opt. Comm. **319**, 14 (2014).
12. M. Kang and Y. D. Chong, Phys. Rev. A **92**, 043826 (2015).
13. P. Yeh, Surf. Sci., **96**, 41 (1980).
14. NiCuNi plated ring magnets, $37 \times 6.5 \times 12$mm, from GaussBoys Super Magnets, Winlock, WA (www.gaussboys.com).

REFERENCES

1. Y. D. Chong, L. Ge, H. Cao, and A. D. Stone, "Coherent Perfect Absorbers: Time-Reversed Lasers," Phys. Rev. Lett., **105**, 053901 (2010).
2. W. Wan, Y. Chong, L. Ge, H. Noh, A. D. Stone, and H. Cao, "Time-Reversed Lasing and Interferometric Control of Absorption," Science, **331**, 889-892 (2011).
3. S. Longhi, "Coherent perfect absorption in a homogeneously broadened two-level medium," Phys. Rev. A **83**, 055804 (2011).
4. S. Dutta-Gupta, O. J. F. Martin, S. Dutta Gupta, and G. S. Agarwal, "Controllable coherent perfect absorption in a composite film," Opt. Express **20**, 1330-1336 (2012).
5. S. Dutta-Gupta and G. S. Agarwal, "Two-photon quantum interference in plasmonics: theory and applications," Opt. Lett. **39**, 390-393 (2014).
6. S. Longhi and G. D. Valle, "Coherent perfect absorbers for transient, periodic, or chaotic optical fields: Time-reversed lasers beyond threshold," Phys. Rev. A **85**, 053838 (2012).
7. K. N. Reddy and S. D. Gupta, "Light-controlled perfect absorption of light," Opt. Lett. **38**, 5252 (2013).
8. S. Longhi, "Non-reciprocal transmission in photonic lattices based on unidirectional coherent perfect absorption," Opt. Lett. **40**, 1278 (2015).
9. M. Crescimanno, N. J. Dawson, and J. H. Andrews, "Coherent perfect rotation," Phys. Rev. A., **86**, 031807(R) (2012).
10. M. Crescimanno, C. Zhou, J. H. Andrews and M. A. Baker, "Structure and symmetry in coherent perfect polarization rotation," Phys. Rev. A **91**. 013845 (2015).
11. Y. Wang, M. Pu, C. Hu, Z. Zhao, C. Wang, and X. Luo, "Dynamic manipulation of polarization states using anisotropic meta-surface," Opt. Comm. **319**, 14 (2014).
12. M. Kang and Y. D. Chong, "Coherent optical control of polarization with a critical metasurface," Phys. Rev. A **92**, 043826 (2015).
13. P. Yeh, "Optics of anisotropic layered media: A new 4×4 matrix algebra," Surf. Sci., **96**, 41-53 (1980).
14. NiCuNi plated ring magnets, $37 \times 6.5 \times 12$mm, from GaussBoys Super Magnets, Winlock, WA (www.gaussboys.com).